Available online at www.sciencedirect.com

ScienceDirect

Procedia CIRP 58 (2017) 445 – 450

www.elsevier.com/locate/procedia

16th CIRP Conference on Modelling of Machining Operations

Discrete Cutting Force Model for 5-Axis Milling with Arbitrary Engagement and Feed Direction

Luke Berglind[a], Denys Plakhotnik[b], Erdem Ozturk[a],*

[a] AMRC with Boeing, the University of Sheffield, Wallis Way, Catcliffe, Rotherham S60 5TZ, United Kingdom
[b] ModuleWorks, Henricistrasse 50, 52072 Aachen, Germany

* Corresponding author. Tel.: +44 (0)114 222 6671; *E-mail address:* e.ozturk@amrc.co.uk

Abstract

5-axis machining operations bring new challenges for predicting cutting forces. Complex tool workpiece engagements and tool orientations make it difficult to adapt 3-axis process models for 5-axis operations. A new model is developed to predict cutting forces with arbitrary tool/workpiece engagement and tool feed direction. A discretization approach is used, in which the tool is composed of multiple cutting elements. Each element is processed to determine its effect on cutting forces, and global forces are determined by combining the elemental effects. Cutting tests are conducted to verify force predictions, where the tool/workpiece engagement is provided through a geometric software application.

Peer-review under responsibility of the scientific committee of The 16th CIRP Conference on Modelling of Machining Operations

Keywords: Milling, Cutting Forces, Discretized Force Model.

1. Introduction

Cutting forces have a direct effect on form errors and surface quality of a machined part. Once cutting forces are simulated, tool and workpiece deflections, which result in form errors and vibrations causing surface quality issues, can be predicted.

Cutting forces depend on the tool and workpiece material, cutting tool geometry and cutting conditions. In 5-axis milling cutting conditions can vary considerably in process, and the varying cutting conditions can result in complex tool-workpiece engagements (TWE). Ozturk and Budak calculated such engagements analytically for 5-axis ball-end milling [1], and also simulated cutting forces throughout a toolpath after calculating the cutting parameters at discrete intervals [2]. Although this method gives accurate results for smooth machining operations, the analytical engagement model loses accuracy when the uncut surface is more complex.

For more accurate force prediction, alternative engagement calculation methods are needed. Several techniques have been developed to model the complex tool/workpiece engagements. These models operate by creating a virtual workpiece, and removing any material that interferes with the geometry of a tool moved along a path. For each tool motion, the surface patches of the tool that remove material are considered to be the TWE region. In the Solid Model based material removal simulation, the engagement area is derived from finding intersections between the solid models of both the tool and the workpiece [3, 4]. Others have represented the workpiece as a Z-map, also known as height map, a matrix/manifold of lines which are virtually cut when they interfere with the tool mesh [5]. A more advanced version of Z-map is the Dexel approach [6] that can model overhangs in the geometry, thus supporting 5-axis milling. The Dexel approach may be improved to so-called tri-Dexel model by introducing virtual grid lines in three directions to reduce dependence on grid directionality in the geometry accuracy for any cut direction. [7, 6, 8]

In the current model, geometric software which applies the tri-Dexel model is used to determine TWE data for every cutter location (CL) point of a part program (see Figure 1).

Peer-review under responsibility of the scientific committee of The 16th CIRP Conference on Modelling of Machining Operations
doi:10.1016/j.procir.2017.03.250

This TWE data determines which elements of a discretized tool mesh are engaged in the cut during that move. The cutting force contribution of each engaged element are then combined to determine the global cutting force for that move.

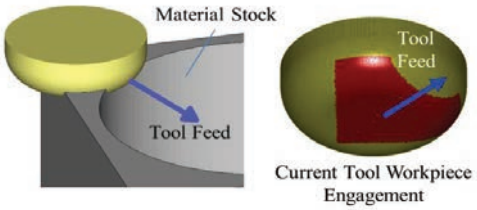

Figure 1: Example tool/workpiece engagement determined through simulation of material removal from stock material.

2. Discretized Force Model

In order to predict cutting forces for arbitrary feed direction with arbitrary TWE, a discrete cutting force model is used. The model concept is shown in Figure 2A, where cutting forces on a bull nose end mill act in different directions based on the cutter position and orientation. An example of the local cutting forces are shown at one section of the cutting edge, where there is a local radial force F_r, acting normal to the cut surface, tangent force, F_t, acting in the opposite direction of the cutting speed, and axial force, F_a, tangent to the cut surface along to the tool profile

The complex cut area from Figure 2B is discretized into multiple elements in Figure 2C. Each element has an effective cut width, b_{el}, and thickness, h_{el}, which represents the cut dimension normal to the cutting edge, **r**. The global tool force is determined by combining the effects of all active cutting elements.

This section outlines the processes to determine the effects each tool element have on global cutting force. Ultimately, the force effects of each element are defined by a constant edge force vector, $F_{e,XYZ,el}$, and a cutting force matrix giving, $F_{c,XYZ,el}$, as a function of tool feed, f_{XYZ}, in Equation (1).

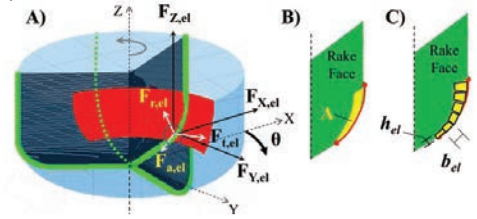

Figure 2: Cutting forces in local radial, tangent, and axial directions for discretized tool elements.

$$\begin{Bmatrix} F_{X,el} \\ F_{Y,el} \\ F_{Z,el} \end{Bmatrix} = \begin{Bmatrix} F_{e,X,el} \\ F_{e,Y,el} \\ F_{e,Z,el} \end{Bmatrix} + \begin{bmatrix} \frac{F_{c,X,el}}{f_X} & \frac{F_{c,X,el}}{f_Y} & \frac{F_{c,X,el}}{f_Z} \\ \frac{F_{c,Y,el}}{f_X} & \frac{F_{c,Y,el}}{f_Y} & \frac{F_{c,Y,el}}{f_Z} \\ \frac{F_{c,Z,el}}{f_X} & \frac{F_{c,Z,el}}{f_Y} & \frac{F_{c,Z,el}}{f_Z} \end{bmatrix} \begin{Bmatrix} f_X \\ f_Y \\ f_Z \end{Bmatrix} \quad (1)$$

$$\{F_{XYZ,el}\} = \{F_{e,XYZ,el}\} + [Q_{XYZ,el}]\{f_{XYZ}\}$$

2.1. Tool Discretization

The tool is discretized circumferentially, and along the tool profile, L, allowing the TWE of the tool to be defined by a single 2D matrix (i.e. it combines radial and axial components into a single vector along the tool profile). In addition, the elements along L are created with equal length, b_{el}, regardless of the orientation of the elements. While other tool geometries can be configured using the current meshing approach, the mesh is illustrated in Figure 3A for a bullnose end mill with tool diameter, D, corner radius, R, and a maximum axial length of Z_{max}.

The mesh is created to follow the helical curve to match the shape of the cutting edge. In Figure 3B, two meshes are shown, one with zero helix angle, and one with λ=30°.

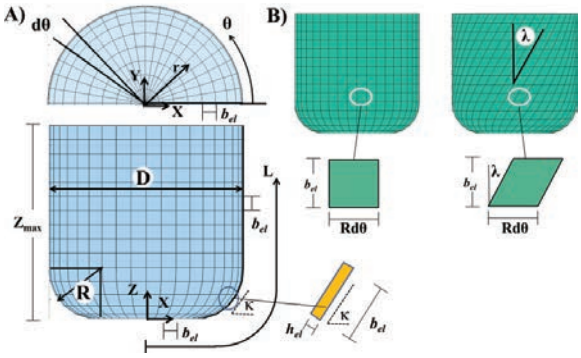

Figure 3: Tool discretisation along the tool profile, L, with increments, b_{el}, at angle, θ, in increments of dθ.

The tool is discretized along the tool profile, L, into N_L elements of dimension b_{el}, and circumferentially into N_c elements with dimensions, dθ. The mesh structure is shown in Figure 4. The L mesh indices represent the concentric circles radiating from the tool tip center and extending up the side of the tool. The element cut width, b_{el}, is the distance between two adjacent L indices. The Θ indices represent the tool elements in the circumferential direction. The circumferential elements are positioned with lag angles to follow the helical curve of the cutting edge, as shown in Figure 4. By creating the mesh along the helical curve, the indices of the TWE Map always correspond directly to the cutting edge, and each Θ index corresponds directly to the elements of one flute at one rotational position.

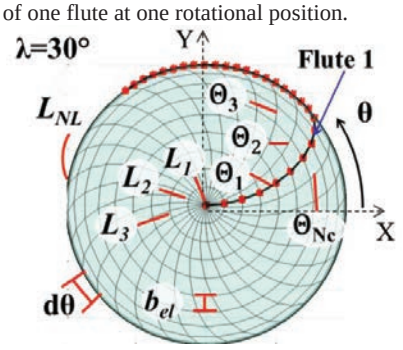

Figure 4: Tool mesh indices following the tool profile, L, and flute position angle, Θ.

Each element of the mesh has the indices, $el(\Theta, L)$, and is defined by a set of position coordinates in Cartesian (X, Y, Z) and polar (R, θ, Z) coordinates, and by an orientation angle, κ (see Figure 3A).

2.2. Tool Coordinate Systems

Three coordinate systems (CS) are used in the cutting force analysis for each element of the cutting edge; **{r t a}**, **{R T A}** and **{X Y Z}**. **{X Y Z}** is the tool global CS, in which tool motions and cutting forces are determined. **{R T A}** is the tool global polar CS, describing radial, tangent and axial directions. **{r t a}** is the local element CS and is used to account for the orientation of the cutting elements. The **rta**-directions correspond to the force directions associated with the cutting force coefficients (CFCs), $K_{e,rta}$ and $K_{c,rta}$, which are fixed relative to the orientation of the cutting element, but change direction based on the element orientation (i.e. side or bottom of the tool profile).

Forces in these three coordinate systems are shown for a single element in Figure 7. Ultimately, forces in the **XYZ** direction are required based on tool feed in the **XYZ** direction, but the cutting forces must first be determined in the **rta** CS in which the cutting force CFCs are defined. Operations required to transform forces from the **rta** CS to the **XYZ** CS, as shown in Figure 5, are discussed in this section.

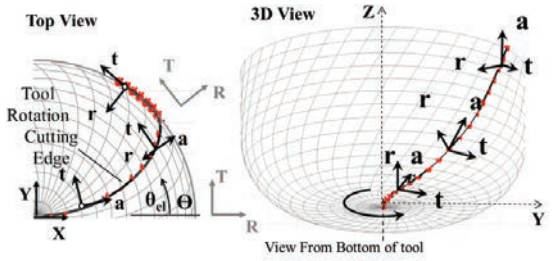

Figure 5: Local and global coordinate systems.

3. Element Cutting Forces

Each tool element will contribute to the global cutting force if it is engaged in the cut. In this section the element cutting forces are first calculated in the local **rta** CS and then transformed to the global tool **XYZ** CS.

3.1. Element Local Cutting Force

Element cutting forces are calculated in the local **rta** CS using Equation (2). In order to determine these element forces for any feed direction, Equation (2) is altered so that the cutting forces are calculated based on the relative feed of that element in the local **rta** directions, f_{rta} (feed per tooth vector in the **rta** directions). By defining the element uncut chip thickness, h_{el}, as a function of the feed vector, it is possible to calculate element forces for any feed direction from a single cutting force matrix for that element. This feature is especially convenient in 5-axis machining where the tool continually changes feed direction.

$$\begin{Bmatrix} F_{r,el} \\ F_{t,el} \\ F_{a,el} \end{Bmatrix} = \begin{Bmatrix} K_{e,r} \\ K_{e,t} \\ K_{e,a} \end{Bmatrix} b_{el} + \begin{Bmatrix} K_{c,r} \\ K_{c,t} \\ K_{c,a} \end{Bmatrix} h_{el} b_{el} \qquad (2)$$

The relationship between the uncut chip thickness and the relative feed of the element, f_{rta}, is illustrated in Figure 6, where h_{el} is equal to the distance that the element is fed in the negative r-direction, f_r (the local **r**-direction vector always points inward, normal to the cut surface). Defining the uncut chip thickness for each element in Equation (3) and combining with Equation (2), the resulting expression for the cutting force for each element is given in Equation (4).

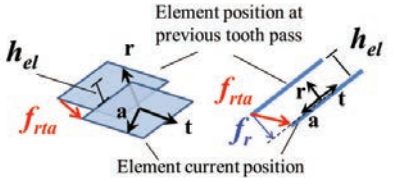

Figure 6: Uncut chip thickness, h_{el}, for a tool element based on the tool feed, f_{rta}, relative to the prior tooth pass.

$$h_{el} = \{-1 \quad 0 \quad 0\} \begin{Bmatrix} f_r \\ f_t \\ f_a \end{Bmatrix} \qquad (3)$$

$$\begin{Bmatrix} F_{r,el} \\ F_{t,el} \\ F_{a,el} \end{Bmatrix} = \begin{Bmatrix} K_{e,r} b_{el} \\ K_{e,t} b_{el} \\ K_{e,a} b_{el} \end{Bmatrix} + \begin{bmatrix} -K_{c,r} b_{el} & 0 & 0 \\ -K_{c,t} b_{el} & 0 & 0 \\ -K_{c,a} b_{el} & 0 & 0 \end{bmatrix} \begin{Bmatrix} f_r \\ f_t \\ f_a \end{Bmatrix}$$

$$\begin{Bmatrix} F_{r,el} \\ F_{t,el} \\ F_{a,el} \end{Bmatrix} = \begin{Bmatrix} F_{e,r,el} \\ F_{e,t,el} \\ F_{e,a,el} \end{Bmatrix} + \begin{bmatrix} \frac{F_{c,r,el}}{f_r} & \frac{F_{c,r,el}}{f_t} & \frac{F_{c,r,el}}{f_a} \\ \frac{F_{c,t,el}}{f_r} & \frac{F_{c,t,el}}{f_t} & \frac{F_{c,t,el}}{f_a} \\ \frac{F_{c,a,el}}{f_r} & \frac{F_{c,a,el}}{f_t} & \frac{F_{c,a,el}}{f_a} \end{bmatrix} \begin{Bmatrix} f_r \\ f_t \\ f_a \end{Bmatrix} \qquad (4)$$

$$\{F_{rta,el}\} = \{F_{e,rta,el}\} + [Q_{rta,el}]\{f_{rta}\}$$

Equation (4) gives cutting forces in the local **rta** CS based on the element feed in in the **rta** directions using the cutting force matrix, $F_{c,rta,el}/f_{rta}$, or $Q_{rta,el}$. The use of $Q_{rta,el}$ is not a significant improvement on Equation (2) in the **rta** CS, however, though simple transformations of $Q_{rta,el}$, this the same force to feed relationship can be applied in any CS.

3.2. Cutting Force Transformations

Cutting forces calculated in Equation (4) must be transformed from the local **rta** CS to the tool **XYZ** CS, as shown in Figure 7.

Two coordinate transformations are required. The first transformation accounts for the local orientation of the cutting edge which is defined by the tool profile angle, κ_{el}. The transformation matrix, $\mathbf{T}_{\kappa el}$, in Equation (5) transforms from the elemental **rta** CS to the tool **RTA** CS.

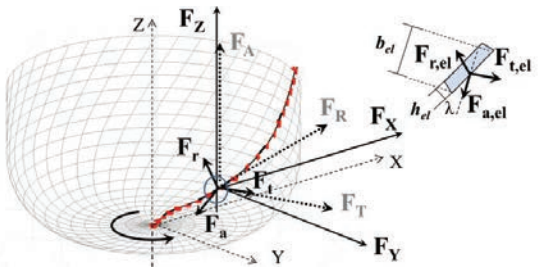

Figure 7: Transformation of the cutting force directions for a single cutting edge element.

$$\mathbf{T}_{\kappa_{el}} = \begin{bmatrix} -sin\kappa_{el} & 0 & -cos\kappa_{el} \\ 0 & 1 & 0 \\ cos\kappa_{el} & 0 & -sin\kappa_{el} \end{bmatrix} \quad (5)$$

The second transformation accounts for the angular position of the element around the tool. The transformation matrix, $\mathbf{T}_{\theta el}$ in Equation (6) transforms from the tool **RTA** CS to the tool **XYZ** CS.

$$\mathbf{T}_{\theta_{el}} = \begin{bmatrix} cos\theta_{el} & -sin\theta_{el} & 0 \\ sin\theta_{el} & cos\theta_{el} & 0 \\ 0 & 0 & 1 \end{bmatrix} \quad (6)$$

Combining (5) and (6), the transformation matrix to transform from the element local **rta** CS to the tool **XYZ** CS is shown in Equation (7).

$$\mathbf{T}_{el} = \mathbf{T}_{\theta_{el}} \mathbf{T}_{\kappa_{el}} \quad (7)$$

Forces in the tool **XYZ** CS are found by performing a coordinate transformation to the edge force vector in (8), and the vector field rotation on the cutting force matrix in (9).

$$\{F_{e,\mathrm{XYZ},el}\} = \mathbf{T_{el}}\{F_{e,rta,el}\} \quad (8)$$

$$[Q_{\mathrm{XYZ},el}] = \mathbf{T_{el}}[Q_{rta,el}]\mathbf{T_{el}^T} \quad (9)$$

The resulting element force vectors, $F_{e,\mathrm{XYZ},el}$, and matrices, $Q_{\mathrm{XYZ},el}$, can then be applied in Equation (1) to determine element forces in **XYZ** based on feed in **XYZ.**

4. Tool Cutting Forces

After transforming in Equations (8) and (9), all of the element force vectors, $F_{e,\mathrm{XYZ},el}$, and matrices, $Q_{\mathrm{XYZ},el}$, share a common CS. Also, at any instant in time (or at any flute position, Θ), all elements of the tool share a common feed, f_{XYZ}. As a result, the global effect of a flute at each position, Θ, can be determined by combining $F_{e,\mathrm{XYZ},el}$ and $Q_{\mathrm{XYZ},el}$ of active elements at each Θ position, as shown in Equation (10)

$$F_{e,\mathrm{XYZ}}(\Theta) = \sum_{L=1}^{N_L} g(\Theta, L) F_{e,\mathrm{XYZ},el(\Theta,L)}$$
$$[Q_{\mathrm{XYZ}}(\Theta)] = \sum_{L=1}^{N_L} g(\Theta, L) [Q_{\mathrm{XYZ},el(\Theta,L)}] \quad (10)$$

The term, $g(\Theta, L)$, in Equation (10) is a matrix of ones and zeros defining which tool mesh elements along the tool profile, L, are engaged in the workpiece at each flute position, Θ. $g(\Theta, L)$ is illustrated in Figure 8 for an example TWE for a 30° helix tool mesh with 30 angular positions, Θ, and 30 elements along the tool profile, L. As the tool rotates, the flute position shifts to different angular positions, and only the elements corresponding to those angular position are engaged at that time. For example, at position Θ_1 in Figure 8 the flute is not in the cut, and $g(\Theta, L) = 0$ for all elements at that position. When the flute is at Θ_{26}, elements 10 through 20 are engaged, and their effects are combined using Equation (10).

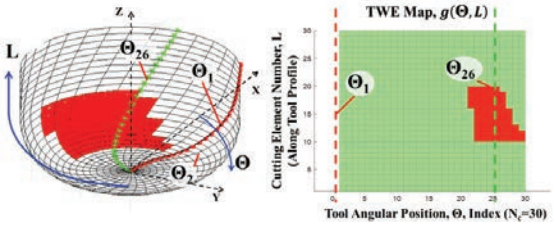

Figure 8: Mesh and TWE indices for a 30° helix cutter.

The global cutting force on the tool for each flute position is determined using Equation (11). Note, if multiple flutes are engaged in the cut at once, the effects of all engaged flutes can also be combined.

$$\{F_{\mathrm{XYZ}}(\Theta)\} = \{F_{e,\mathrm{XYZ}}(\Theta)\} + [\boldsymbol{Q}_{\mathbf{XYZ}}(\Theta)]\{f_{\mathrm{XYZ}}\} \quad (11)$$

Cutting forces are determined by evaluating Equation (11) for each flute position. As the tool rotates through the different positions, the components of Equation (11) change to reflect the engaged elements in that section.

The example in Figure 9 shows the calculated cutting forces for a 12mm diameter ball-end mill with full radial immersion with a cutting depth of 3mm. For this cut, the tool is fed in the negative Y-direction at a rate of 0.1mm per tooth, so the feed vector is constant at $f_{\mathrm{XYZ}} = \{0, -0.1,\ 0\}^T$. Equation (11) is then evaluated at each position (only positions 1 through 7 are shown), to obtain the changing cutting forces as the tool rotates through the engagement region.

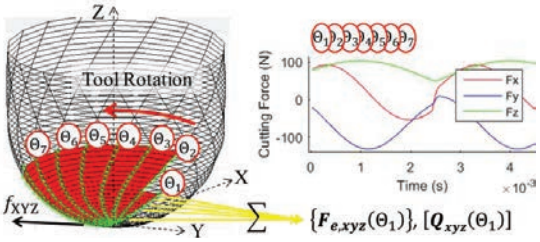

Figure 9: Calculation of cutting forces with a single operation for each global rotation angle by combining all active cutting elements at that angle.

5. Part Cutting Forces

In 5-axis machining the orientation of the tool can change continually with respect to the workpiece. So far cutting forces have been determined in the tool CS. However, cutting forces in the part CS, $\mathrm{XYZ_P}$, based on tool feed in

XYZ_P are often more convenient as tool motions are programed in the part CS. After transforming $F_{e,\mathrm{XYZ}}(\Theta)$ and $\boldsymbol{Q}_{\mathbf{XYZ}}(\Theta)$ in Equation (12) based on the coordinate transformation from the tool CS to the part CS, TT2P, cutting forces are obtained in the part CS using Equation (13).

$$\begin{aligned}\{F_{\mathrm{XYZ}_P}(\Theta)\} &= \mathbf{T_{T2P}}\{F_{e,\mathrm{XYZ}}(\Theta)\} \\ [\boldsymbol{Q}_{\mathbf{XYZ}_P}(\Theta)] &= \mathbf{T_{T2P}}[\boldsymbol{Q}_{\mathbf{XYZ}}(\Theta)]\mathbf{T}_{\mathbf{T2P}}^{\boldsymbol{T}}\end{aligned} \quad (12)$$

$$\{F_{\mathrm{XYZ}_P}(\Theta)\} = \{F_{e,\mathrm{XYZ}_P}(\Theta)\} + [\boldsymbol{Q}_{\mathbf{XYZ}_P}(\Theta)]\{f_{\mathrm{XYZ}_P}\} \quad (13)$$

6. Cutting Experiments

Two cutting tests are performed to compare simulated and measured cutting forces. The tool for both tests is a 12mm diameter ball-end mill with two flutes and helix angle of 30°. The machine used for the tests is a MAG FTV5-2500 and force measurements are collected using a Kistler 9139AA dynamometer. The CFCs used for the AL7075-T6 workpiece are found experimentally using a ball end mill mechanistic model [9], to be: $K_{e,r}$=13.9, $K_{e,t}$=7.1, $K_{e,a}$=-1.3 N/mm, and $K_{c,r}$=619.9, $K_{c,t}$=1014.2, and $K_{c,a}$=58.2 N/mm^2. Note that average CFC values identified experimentally are used for all elements regardless of local oblique and rake angles.

The first test is a stair step test where the axial depth increases from 1 to 3 mm in increments of 0.25 mm, with full radial immersion and zero lead and tilt. For this test, the spindle speed is 10,000 RPM with a feed rate of 0.1 mm per tooth. The force measurements in the part CS, F_{XYZP}, are shown in Figure 10, along with the maximum and minimum simulated forces. A detailed comparison of the simulated and measured cutting forces is also shown in Figure 10 for the minimum depth of 1 mm and maximum depth of 3 mm. It can be seen from these results that the simulated results closely match the experiment for this simple operation.

The second test is on the "M" part shown in Figure 11, which is machined at 12250 RPM using approximately 850 CL points. During this test, the A and C axes of the machine are fixed at 21.1° and -134°, respectively, resulting in a lead and tilt of 15° when feeding in the $-X_P$ feed direction on the XY_P plane. The rotary axes are fixed to reduce tracking errors between the simulation and the true machine motions. This part is machined over a dome shaped base which results in varying depth over the "M" profile. Further, the fixed tool orientation results in a fixed transformation, $\mathbf{T_{T2P}}$, but variable lead and tilt angle as the tool changes direction.

Prior to the start of the simulation, the tool mesh is created, and $F_{e,\mathrm{XYZ},el}$ and $Q_{\mathrm{XYZ},el}$ are determined for each tool mesh element (these only need to be calculated once for a given tool mesh and fixed set of cutting force coefficients). Then, for each CL point, the TWE is obtained for that move using geometric software which applies a tri-Dexel model. Figure 11 shows examples of how the TWE maps obtained change throughout the operation. The TWE data for each move then applied to obtain $F_{e,\mathrm{XYZ}}(\Theta)$ and $Q_{\mathrm{XYZ}}(\Theta)$, and the cutting forces are calculated using Equation (11) at each angular position.

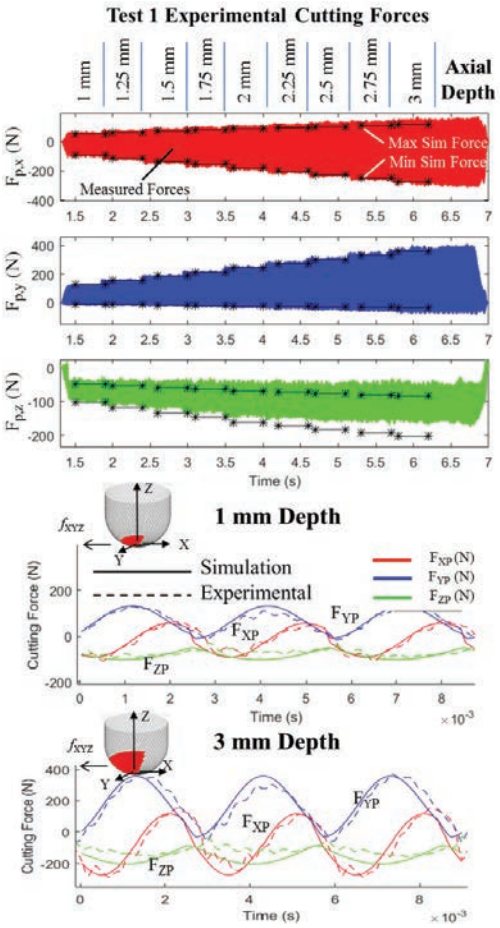

Figure 10: Step cutting force test results for Test 1 (zero lead and tilt) showing detailed comparison of the simulated force results for A) 1mm depth and B) 3mm depth.

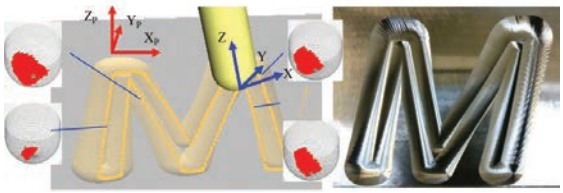

Figure 11: Test cut "M" character with varying cut depth.

Due to tracking errors in the tool feed velocity (despite fixing the A and C axes), the total machining time is approximately 20% longer than expected. To account for this in the simulation, the feed per tooth was reduced to 0.078 mm per tooth to match the actual and simulation machine time (this effectively reduced the simulated average tool speed).

The resulting forces are plotted in Figure 12 along with the maximum and minimum simulated force values at those locations in time. The results show that the simulated maximum and minimum forces closely follow the force profile throughout the operation. The only places where large deviations occur are in locations where chatter occurs,

as expected. Further, the simulated rotation dependent forces in Figure 13 also closely match the measured forces.

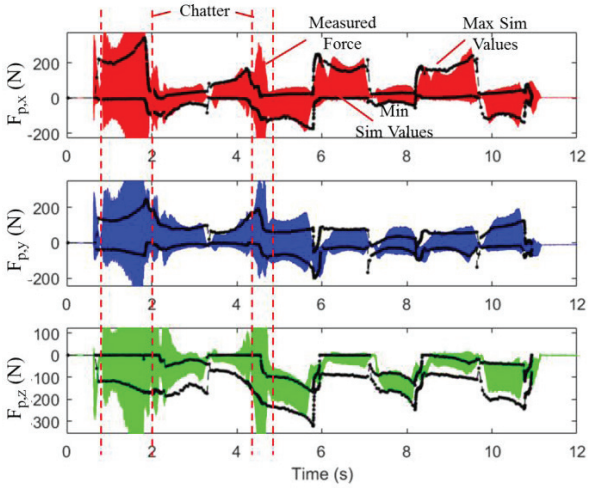

Figure 12: Measured forces in workpiece CS with maximum and minimum simulated force values at each corresponding location.

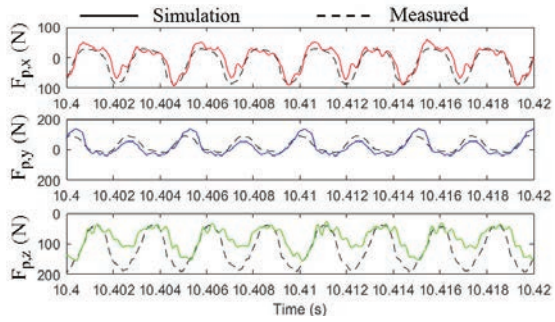

Figure 13: Comparison of simulated and measured force data at one location of the "M" part.

7. Conclusions

The cutting force model developed in this paper was created to predict forces for complex machining operations where the tool/workpiece engagement is complex and highly variable throughout. The key feature of this model is that it treats the elements of a discretized tool as individual entities which have predetermined force characteristics ($F_{e,\mathrm{XYZ},el}$ and $Q_{\mathrm{XYZ},el}$) which depend on the feed direction of the tool. When coupled with geometric software to capture effect of changing cutting conditions on the TWE, it is possible to efficiently obtain complex cutting force predictions for 5-axis operations.

The experiments discussed here have shown that this model is capable of predicting cutting force for a ball end mill in 3 and 5-axis operations. The stair test resulted in accurate predictions of cutting force at varying cut depths. The "M" test demonstrated that this model is able to pair with geometric software and account for a high variation of cutting conditions effectively. The predictions from this test showed close agreement between simulated and measured forces.

Acknowledgements

The authors would like to acknowledge the support from European Union Horizon 2020 project, Twin-Control, for this research (grant agreement No. 680725).

References

[1] E. Ozturk and E. Budak, "Modelling of 5-axis Milling Processes," *Machining Science and Technology*, pp. 11:3, 287–311, 2007.

[2] E. Budak, E. Ozturk and L. T. Tunc, "Modelling and simulation of 5-axis milling processes," *Machining Science and Technology*, pp. 287-311, 2007.

[3] I. Lazoglu, Y. Boz and H. Erdim, "Five-Axis Milling Mechanics for Complex Free From Machining," *CIRP Annals - Manufacturing Technology*, pp. 60:117-120, 2011.

[4] Y. Boz, H. rdim and I. Lazoglu, "Modeling Cutting Forces for 5-Axis Machining of Sculptured Surfaces," in *2nd International Conference, Process Machine Interactions*, 2010.

[5] G. Kim, P. Cho and C. hu, "Cutting force prediction of sculptured surface ball-end milling using Z-map," *International Journal of Machine Tools & Manufacture*, vol. 40, p. 277–291, 2000.

[6] V. Boess, C. Ammermann, D. Niederwestberg and B. Denkena, "Contact Zone Analysis Based on Multidexel Workpiece Model and Detailed Tool Geometry representation," in *3rd CIRP Conference on Process Machine Interactions*, 2012.

[7] K. Erkorkmaz, A. K. Y. Hosseinkhani, D. Plakhotnik, M. Stautner and F. Ismail, "Chip geometry and cutting forces in gear shaping," *CIRP Annals - Manufacturing Technology*, pp. 133-136, 2016.

[8] T. Siebrecht, P. Kersting, D. Biermanna, S. Odendahla and J. Bergmann, "Modeling of surface location errors in a multi-scale milling simulation system using a tool model based on triangle meshes," in *CIRPe 2015 - Understanding the life cycle implications of manufacturing*, 2015.

[9] J. Gradisek, M. Kalveram and K. Weinert, "Mechanistic Identification of Specific Force Coefficients for a General End Mill," *International Journal of Machine Tools and Manufacture*, vol. 44, pp. 401-414, 2004.

[10] Y. Altintas, Manufacturing Automation; Metal Cutting Mechanics, Machine Tool Vibrations, and CNC Design, 2nd Edition, Cambridge University Press, 2012.

[11] S. Layegh, H. Erdim and I. Lazoglu, "Offline Force Control and Feedrate Scheduling for Complex Free Form Surfaces in 5-Axis Milling," in *CIRP Conference on High Performance Cutting*, 2012.

[12] L. M. Kumanchik and T. L. Schmitz, "Improved analytical chip thickness model for milling," *Precision Engineering 31*, p. 317–324, 2007.

[13] T. L. Taner, Ö. Ömer and B. Erhan, "Generalized cutting force model in multi-axis milling using a new engagement boundary determination approach," *Int J Adv Manuf Technol*, pp. 77:341-355, 2015.